PERGAMON

International Journal of Heat and Mass Transfer 43 (2000) 353–364

International Journal of HEAT and MASS TRANSFER

www.elsevier.com/locate/ijhmt

Pressure-driven water flows in trapezoidal silicon microchannels

Qu Weilin, Gh. Mohiuddin Mala, Li Dongqing*

Department of Mechanical Engineering, 4–9 Mechanical Engineering Building, University of Alberta, Edmonton, Alberta, Canada T6G 2G8

Received 5 November 1998; received in revised form 23 April 1999

Abstract

Experiments were conducted to investigate flow characteristics of water through trapezoidal silicon microchannels with a hydraulic diameter ranging from 51 to 169 μm. In the experiments, the flow rate and pressure drop across the microchannels were measured at steady states. The experimental results were compared with the predictions from the conventional laminar flow theory. A significant difference between the experimental data and the theoretical predictions was found. Experimental results indicate that pressure gradient and flow friction in microchannels are higher than those given by the conventional laminar flow theory. The measured higher pressure gradient and flow friction maybe be due to the effect of surface roughness of the microchannels. A roughness–viscosity model is proposed to interpret the experimental data.

1. Introduction

The rapid development of MEMS and micro-fluidic devices has generated an increasing demand for understanding of liquid flows in microchannels or microchannel structures. The liquid flow characteristics in microchannels are important in the design and the process control of MEMS and micro-fluidic devices. It has been found that for fluid flow in microchannels, the flow behavior often deviate significantly from the predictions of conventional theories of fluid mechanics.

Wu and Little [15] measured the friction factors for the flow of gases in the miniature channels. The test channels were etched in glass and silicon with hydraulic diameter ranging from 55.81 to 83.08 μm. The tests involved both laminar and turbulent flow regimes. They found that the friction factors for both flow regimes in these channels were larger than predictions from the established correlations for macroscale pipes. A transition Reynolds number to turbulent flow can be as low as 350. They attributed these deviations to the relatively high surface roughness, asymmetric roughness and uncertainty in the determination of the channels dimensions.

Harley and Bau [4] measured the friction factors in microchannels with trapezoidal and rectangular cross-sections. The trapezoidal microchannel has dimensions of 33 μm (depth), 111 μm (top width) and 63 μm (bottom width), and the rectangular one has dimensions of 100 μm in depth and 50 μm in width. They found that the product $f \cdot Re$ ranged from 49 for the rectangular channel to 512 for the trapezoidal channel in contract to the classical value of 48.

Choi et al. [1] measured friction factors for flow of nitrogen gas in microtubes for both the laminar and turbulent regimes. The internal diameter of these microtubes ranges from 3 to 81 μm. The relative

* Corresponding author. Tel: +780-492-9734; fax: +780-492-2200.

E-mail address: dongqing.li@ualberta.ca (D. Li)

0017-9310/00/$ - see front matter
PII: S0017-9310(99)00148-9

Nomenclature

A	empirical coefficient in Eq. (16)
A_c	cross-sectional area of the microchannel
A_s	surface area of the microchannel
C_1, C_2, C_3, C_4	coefficients in Eq. (10)
C_f	friction factor constant, $C_f = f \cdot Re$
C^*	friction factor constant ratio, Eq. (14)
DIUF	deionized ultra-filtered water
F	body force vector
J	Jacobi determinant
K	loss coefficient
L	length of the microchannel
P	pressure vector
P_c	perimeter of the microchannel
ΔP	pressure drop across the microchannel
ΔP_{loss}	pressure losses at the inlet and outlet of the microchannel
P_x	pressure gradient in x-direction
Q	volume flow rate
R_h	hydraulic radius of the microchannel, that is, half of the hydraulic diameter d_h
Re	Reynolds number
Re_k	Reynolds number based on the roughness, Eq. (17)
RVM	roughness-viscosity model
U_k	velocity at the top of the roughness element
a, b, h	dimensions of the trapezoidal microchannel
d_h	hydraulic diameter of the channel, that is, ratio of four times of the cross-sectional area to the wetted perimeter of the channel
f	Blasius friction factor or friction factor, $f = \frac{2d_h}{\rho u_m^2}\left(-\frac{dP}{dx}\right)$
f_F	Fanning friction factor, $f = \frac{d_h}{2\rho u_m^2}\left(-\frac{dP}{dx}\right)$
l_{min}	shortest distance from the point to the silicon surface of the microchannel
k	height of the roughness element
n	outer normal coordinate at a point on the microchannel wall inside periphery Γ
t	time
u	velocity vector
u, v, w	velocity in the x, y, z direction respectively
u_m	average velocity
w_x	uncertainty of variable x
x, y, z	Cartesian coordinates

Greek symbols

η, ζ	transformed computational coordinates
ϕ	apex angle of the trapezoidal microchannel
μ	dynamic viscosity of water
μ_R	roughness viscosity
ρ	density of water
Γ	inside periphery of the microchannel wall

Subscripts

exp	experimentally determined value
thy	theoretically determined value

roughness of these microtubes ranges from 0.00017 to 0.016. They found the measured friction factors in laminar flow are less than those predicted from the macro tube correlations, e.g., the friction factor constant, $f \cdot Re$, has a value of 53, instead of 64. The friction factors in turbulent flow are also smaller than those predicted by conventional correlations. No roughness dependence was observed.

Pfahler [11] measured the friction coefficient or apparent viscosity of isopropanol alcohol and silicon oil in microchannels, and found that the apparent viscosity becomes smaller as the channel size decreased. However, there is a good agreement between the experimental results and the predictions of the classical theory for larger channels.

Peng et al. [10] experimentally investigated the flow characteristics of water flowing through rectangular microchannels with hydraulic diameters ranging from 0.133 to 0.367 mm and width to height ratios from 0.333 to 1. Their experimental results indicated that the flow transition occurs at Reynolds number 200–700. This transitional Re decreases as the size of the microchannel decreases. The flow friction behaviors of both the laminar and turbulent flows were found to depart from the classical correlations. The friction factors are either larger or smaller than the predictions of the classical theories. The geometrical parameters, such as hydraulic diameter and the aspect ratio, were found to have important effects on flow.

Yu et al. [16] studied the fluid flow and heat transfer characteristics of dry nitrogen gas and water in microtubes with diameters of 19, 52 and 102 μm. The Reynolds number in their study ranges from 250 to over 20 000. The average relative roughness for 52 μm microtube was measured and the value is approximately 0.0003. The flow friction results indicate that

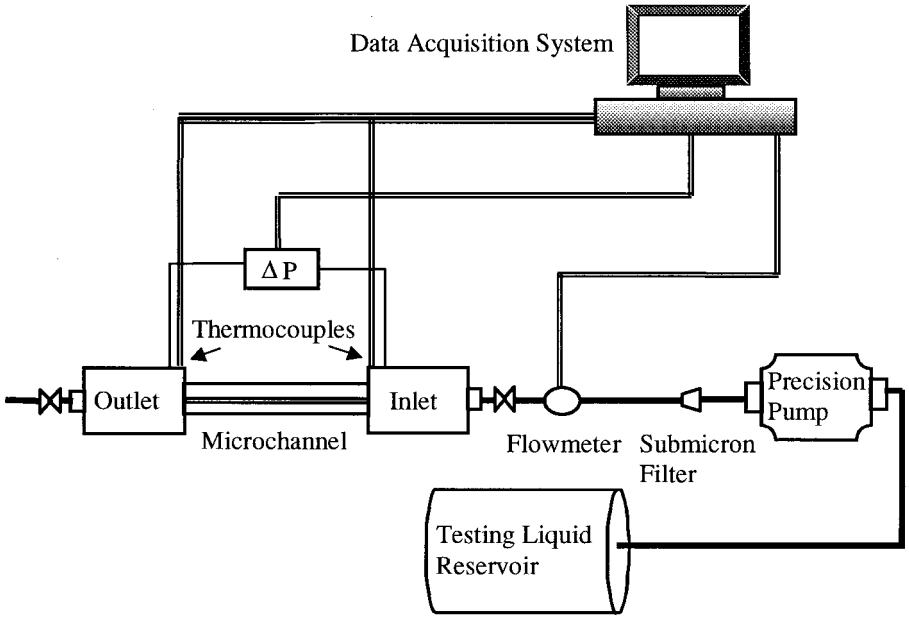

Fig. 1. Schematic of the experimental system for measuring liquid flow in microchannels.

for laminar flow in microtubes, the value of the product, $f \cdot Re$, is between 49.35 and 51.56, instead of 64. A similar, but smaller reduction in the friction factor was observed for both the transitional and the turbulent regimes in the microtubes.

Flockhart and Dhariwal [3] measured the flow characteristics of distilled water in trapezoidal microchannels with a hydraulic diameter ranging from 50 to 120 μm. The investigation were kept within the laminar flow regime for Reynolds number up to 600. For comparison, a numerical technique is employed to predict the flow characteristics. They found that the numerical analysis based on conventional fluid mechanics can adequately predict the flow characteristics of water in trapezoidal microchannels.

Mala and Li [7] measured pressure gradients of water flow in microtubes with inner diameter ranging from 50.0 to 254.0 μm. The Reynolds number was up to 2100. They found for larger microtubes with inner diameter above 150 μm, the experimental results were in rough agreement with the conventional theory. For smaller microtubes, the pressure gradients are up to 35% higher than these predicted by the conventional theory. Furthermore, as *Re* increased, the differences between the experimental results and the conventional theory predictions also increased. They suspected that these effects were either due to change in the flow mode, from laminar to turbulent at lower Reynold numbers, or due to the effects of surface roughness.

Our current understanding to these special flow behaviors is far from sufficient. It is necessary to carry out fundamental investigations to understand the difference between the experimental data and the conventional theory. The objective of this work is to experimentally investigate the characteristics of water flow in trapezoidal microchannels made in silicon plates and attempt to explain the experimental results.

2. Experimental setup and procedures

A schematic of the experimental apparatus used to investigate fluid flow in trapezoidal silicon microchannels is shown in Fig. 1. Deionized ultra filtered water (DIUF) (Fisher Scientific) at the room temperature was used as the working fluid. Water was pumped from the liquid reservoir by a high precision pump (Ruska Instruments, Model: 2248-WII) which has a flow rate range of 2.5–560 cm^3/hr and can generate a pressure up to 4000 psi. In order to avoid any particles or bubbles from flowing through and blocking the microchannels, a 0.1 μm filter was installed between the outlet of the pump and the inlet of the microchannels, and water was forced to flow through the submicron filter before entering the microchannel. The volume flow rate of water flowing through the microchannels was measured by a precision flow meter (CHEM TEC, model: MAO-125 AA). The flow meter is designed for low flow rate (up to 70 cm^3/min) and was calibrated by the standard weighting method as follows. Basically, the liquid exiting the channel was accumulated in a glass beaker. An electronic balance

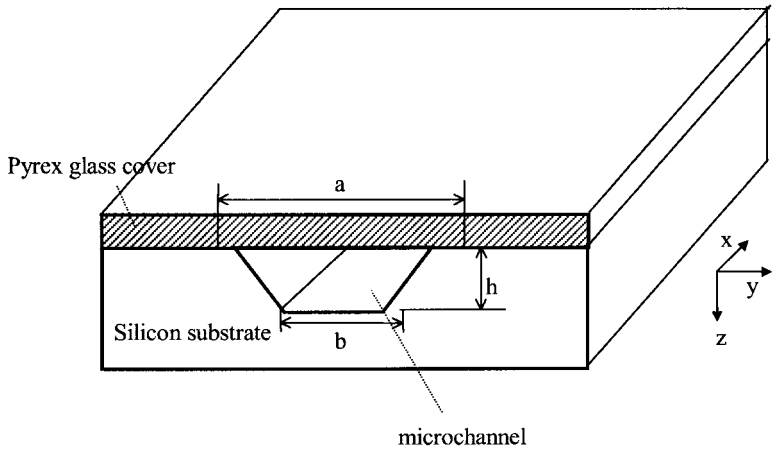

Fig. 2. Schematic of a trapezoidal microchannel in a silicon plate with a Pyrex glass cover.

(METTLER INSTRUMENTE AG, model: BB240) with an accuracy of 0.001 g was used to measure the weight of the accumulated liquid. The volume of the liquid was determined by dividing the weight by the liquid's density. Details of the calibration is given in Mala's Ph.D. thesis [8]. The accuracy of the flow rate measurement was estimated to be 2%.

The trapezoidal silicon microchannels used in this work were fabricated by anisotropic etching technique at Alberta Microelectronic Center (Edmonton, Canada). First several microchannels were etched in a silicon plate and then a Pyrex glass plate was anodically bonded on the top of the plate. The microchannel plates used in the measurement have a dimension of $30 \times 10 \times 1\ \text{mm}^3$. There are five microchannels in each plate. The microchannels in one plate have the same dimensions so that the flow through each channel is identical. The cross-section of such a microchannel is illustrated in Fig. 2. The dimensions of the microchannels were measured by a microscope (Leica MS5 Stereomicroscope) with a resolution of 0.8 μm. The characteristic sizes are listed in Table 1. The hydraulic diameter of the microchannels used in this study ranges from 51 to 169 μm.

The microchannel plate was placed in a two-part symmetrical Plexiglas assembly, as shown in Fig. 3. The epoxy resin was used to bond the microchannel plate and the assembly together to avoid leaking. Two sumps were machined in the assembly and were connected by microchannels. A diaphragm type differential pressure transducer (Validyne Engineering, Model: DP15) with $\pm 0.5\%$ FS accuracy was connected to the sumps to measure the pressure drop along microchannels. In order to provide high accuracy, pressure transducers for different pressure ranges were employed. All the pressure transducers were calibrated by using a standard deadweight pressure source before used in the experiments. The details of the calibration procedures and the results are given in Mala's Ph.D. thesis [8].

The inlet and outlet losses of the microchannels were estimated by the following equations.

Table 1.
Characteristic dimensions of the trapezoidal silicon microchannels[a]

Channel. No.	a (μm)	b (μm)	h (μm)	d_h (μm)	k (μm)
1	405.27	359.72	28.06	51.3	0.8
2	148.33	94.83	44.44	62.3	0.8
3	162.11	105.43	45.47	64.9	0.8
4	237.01	66.11	109.77	114.5	2.0
5	318.81	150.24	113.84	142.0	2.0
6	523.20	356.32	111.14	168.9	2.0

[a] Length of the microchemicals = 2.8 cm and number of microchannels per plate = 5.

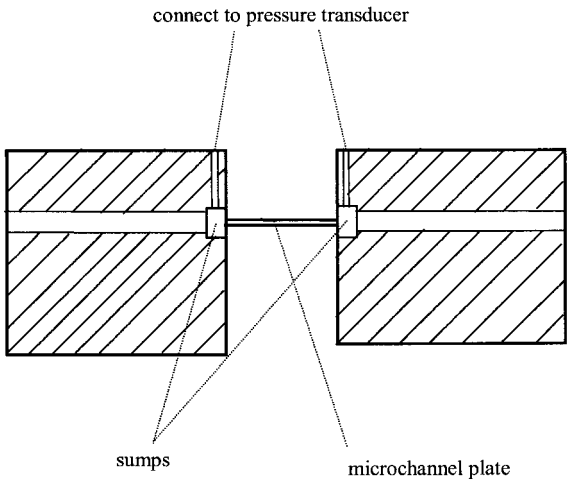

Fig. 3. Schematic of the test section.

$$\Delta P_{\text{loss}} = K\frac{\rho u_{\text{m}}^2}{2} = K\frac{\rho Q^2}{2A_{\text{c}}^2} \tag{1}$$

where K is the loss coefficient. For microchannel inlet, K takes 1.0, and for outlet K takes 0.5 ([13]). The real pressure drop ΔP along the microchannel was obtained by subtracting the inlet and outlet losses from the pressure transducer reading. Realizing that Eq. (1) is used to estimate the maximum pressure loss involved when fluid flow through the entrance and exit of the channel ([2]), therefore, Eq. (1) may give overestimated values for inlet and outlet losses.

In order to determine physical properties of the fluid, two T-type copper constantan thermocouples (Omega Engineering) were placed at the sumps to measure the inlet and outlet temperature of the liquid. All the measurements reported in this paper were done at a temperature of approximately 25°C.

All the measurement devices were connected to the computer data acquisition system. During a measurement, the pump was set to maintain a desired flow rate and the pressure drop along the microchannel was measured. For each measurement, the flow was considered to have reached a steady state when the readings of the pressure drop did not change any more. At such a steady state, the pressure drop and the flow rate were monitored and recorded for about 30 min. The data reported in this paper are for steady states. The measurement for the same microchannel was repeated at least twice for the same flow rate. Then another set of measurement at a different flow rate was conducted for the same microchannel. For every microchannel, the test was conducted up to a pressure drop of 250 psi, as microchannel failure (breaking) usually occurred at pressures drop greater than 250 psi. Therefore, this limited the Reynolds number range to only a few hundreds for smaller microchannels.

Table 2
Experimental uncertainties

Parameters	Uncertainty (%)
Flow rate	2.0
Pressure drop	1.0
Inlet and outlet temperatures	0.8
Pressure gradient	1.4
Reynolds number	4.6
Friction factor	7.6

The uncertainties involved in the measurements were analyzed and evaluated. The results are given in Table 2. The detailed experimental uncertainty analysis can be found in Appendix. For graphic reasons, the error bars were not shown in all the plots reported in this paper.

3. Results and discussion

During the experiments, the measured parameters were the volume flow rate Q and the pressure drop across the microchannel ΔP. Other parameters used to describe the flow characteristics of water, such as pressure gradient P_x, Reynolds number Re, friction factor f, and friction factor constant C_{f}, can be easily related to these two measured parameters as follows.

$$P_x = \frac{\Delta P}{L} \tag{2}$$

$$Re_{\text{exp}} = \frac{\rho Q d_{\text{h}}}{A_{\text{c}}\mu} \tag{3}$$

$$f_{\text{exp}} = \frac{2\Delta P d_{\text{h}} A_{\text{c}}^2}{L\rho Q^2} \tag{4}$$

$$C_{\text{f}_{\text{exp}}} = f_{\text{exp}} \cdot Re_{\text{exp}} \tag{5}$$

The physical properties of water involved in these calculations, such as density ρ, dynamic viscosity μ, were determined from the measured water temperature and were assumed independent of the pressure. In the following sections, the experimental results are first compared with the predictions of the conventional theory for fully developed laminar flow; then the special flow characteristics of water in the microchannels are discussed; finally a rough-viscosity model is proposed to explain the observed phenomena.

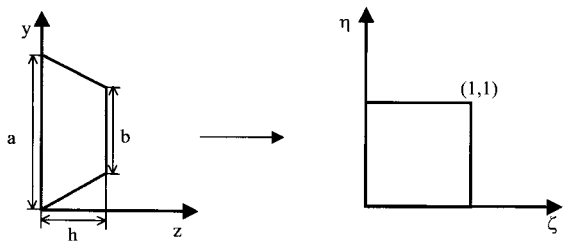

Fig. 4. Schematic of the transformation of a trapezoid in Cartesian coordinates to a square in the computational coordinate.

3.1. Conventional theory

Consider a laminar flow of an incompressible viscous liquid in a two-dimensional trapezoidal microchannel as shown in Fig. 2. The equations of motion is given by:

$$\rho\frac{\partial \mathbf{u}}{\partial t}+\rho(\mathbf{u}\cdot\nabla)\mathbf{u}=-\nabla\mathbf{P}+\mathbf{F}+\mu\nabla^2\mathbf{u} \tag{6}$$

For a fully developed flow at steady state, the equations of motion can be further simplified. Since the flow has no velocity components normal to the x direction, v and w are zero and $u=u(y,z)$ in terms of the cartesian coordinates as shown in Fig. 2. For a fully developed steady state flow, $\partial w/\partial t=0$, $\partial u/\partial x=0$ and $\partial P/\partial x=\text{const}$.

Furthermore, the effect of the body force F is assumed negligible. Under these conditions, Eq. (6) reduces to

$$\frac{\partial^2 u}{\partial y^2}+\frac{\partial^2 u}{\partial z^2}=\frac{1}{\mu}\frac{\mathrm{d}P}{\mathrm{d}x} \tag{7}$$

The boundary condition on the wall is the no-slip condition, given as

$$u(y,z)=0 \text{ on } \Gamma \tag{8}$$

Eq. (7) is a two-dimensional, second-order partial differential equation. Once it is solved with the boundary condition for a given pressure gradient, the velocity field in the microchannels can be determined. However, since the microchannel has a trapezoidal cross-section, an analytical solution for Eq. (7) is not possible and a numerical method has to be employed.

A numerical finite difference scheme was developed here to discretize the governing equation, Eq. (7). However, it should be noted that the cross-section geometry of the microchannel is trapezoidal. This will result in a non-uniform grid system and it is difficult and inefficient to work with. Therefore, a transformation was made to convert the trapezoidal cross-section into a square or rectangular cross-section before the finite difference scheme can be employed. This was achieved by a coordinate system transformation given as

Table 3.
Numerical results of friction constant for microchannels used in this study

Channel No.	ϕ (degrees)[a]	b/h	$f\cdot Re$
1	50.94	12.82	84.880
2	58.95	2.13	60.696
3	58.07	2.32	61.624
4	52.10	0.60	52.084
5	53.48	1.32	55.412
6	53.10	3.21	65.196

[a] ϕ is the apex angle of the trapezoidal channel.

$$\eta=\frac{2hy-(a-b)z}{2ha-2(a-b)z} \tag{9a}$$

$$\zeta=\frac{z}{h} \tag{9b}$$

In this way, the trapezoidal cross-section of the microchannel in the y–z coordinate system can be converted to a square cross-section in the η–ζ coordinate system as shown in Fig. 4. The equation of motion, Eq. (7), should also be re-written in terms of the transformed computational coordinate system. The final form of the transformed equation of motion is expressed as

$$C_1\frac{\partial^2 u}{\partial\zeta^2}+C_2\frac{\partial^2 u}{\partial\eta^2}+C_3\frac{\partial^2 u}{\partial\zeta\partial\eta}+C_4\frac{\partial u}{\partial\eta}=\frac{J}{\mu}\frac{\mathrm{d}P}{\mathrm{d}x} \tag{10}$$

where J is a Jacobi determinant,

$$J=\begin{vmatrix}\dfrac{\partial z}{\partial\zeta} & \dfrac{\partial z}{\partial\eta}\\ \dfrac{\partial y}{\partial\zeta} & \dfrac{\partial y}{\partial\eta}\end{vmatrix}=ah-(a-b)h\zeta \tag{11}$$

C_1, C_2, C_3 and C_4 are coefficients in the Eq. (10). For the transformation given by Eq. (9a), they can be expressed as

$$C_1=\frac{a}{h}-\frac{a-b}{h}\zeta \tag{12a}$$

$$C_2=\frac{h^2+(a-b)^2\left(\eta^2-\eta+\dfrac{1}{4}\right)}{ah-(a-b)h\zeta} \tag{12b}$$

$$C_3=\frac{a-b}{h}(2\eta-1) \tag{12c}$$

Table 4
Comparison of numerical results with results of Shah and London [12] for trapezoidal channels

ϕ (degrees)	b/h	$f \cdot Re$ (Shah and London)	$f \cdot Re$ (this work)
45	8.0	78.972	78.935
	4.0	69.588	69.687
	2.0	60.824	60.850
	1.33	57.040	57.077
	1.0	55.308	55.281
	0.75	54.164	54.176
	0.5	53.456	53.495
60	8.0	81.216	81.202
	4.0	72.212	72.241
	2.0	62.772	62.765
	1.33	58.548	58.545
	1.0	56.604	56.605
	0.75	55.552	55.568
	0.5	55.216	55.281

$$C_4 = \frac{(a-b)^2(2\eta-1)}{ah-(a-b)h\zeta} \tag{12d}$$

A finite difference scheme was applied to Eq. (10), and the resulting system of algebraic equations was solved using the Gauss–Seidal iterative technique, with successive over-relaxation employed to improve the convergence time. In this way, the theoretical velocity distribution across the microchannel cross-section was determined. In order to verify our numerical results, our numerical solution was compared with other solutions. For various shapes of the channel cross-section, a very good agreement was found, which provided confidence in our numerical method. For example, for channels with square cross-sections, the friction factor constant C_f is calculated to be 56.92 from our numerical method, which is in excellent agreement with the value of 57 from the conventional theory. Table 3.lists the numerical results of the friction factor constants for channels used in this study. For comparison, the friction factor constants given by Shah and London [12] for trapezoidal channels with similar geometry and the results of our corresponding numerical solutions are shown in Table 4. It can be seen from Table 4, our results are very close to those given by Shah and London [12]. It should be noted that the friction factors used in Shah and London's book were Fanning friction factor, which was defined as

$$f_F = \frac{d_h}{2\rho u_m^2}\left(-\frac{dP}{dx}\right) \tag{13}$$

For consistency, the friction factors used in Table 4 are converted to Blasius friction factors which are four times of Finning friction factors [6].

In this paper, the theoretical predictions of the flow characteristics in microchannels are obtained follow this way. The measured pressure drop and the real microchannel dimensions were first employed to calculate the velocity field in the microchannel by means of the numerical method described above; then other useful parameters, such as the average velocity u_m, flow rate Q, Reynolds number Re, friction factor f, and friction factor constant C_f, were determined from the velocity field.

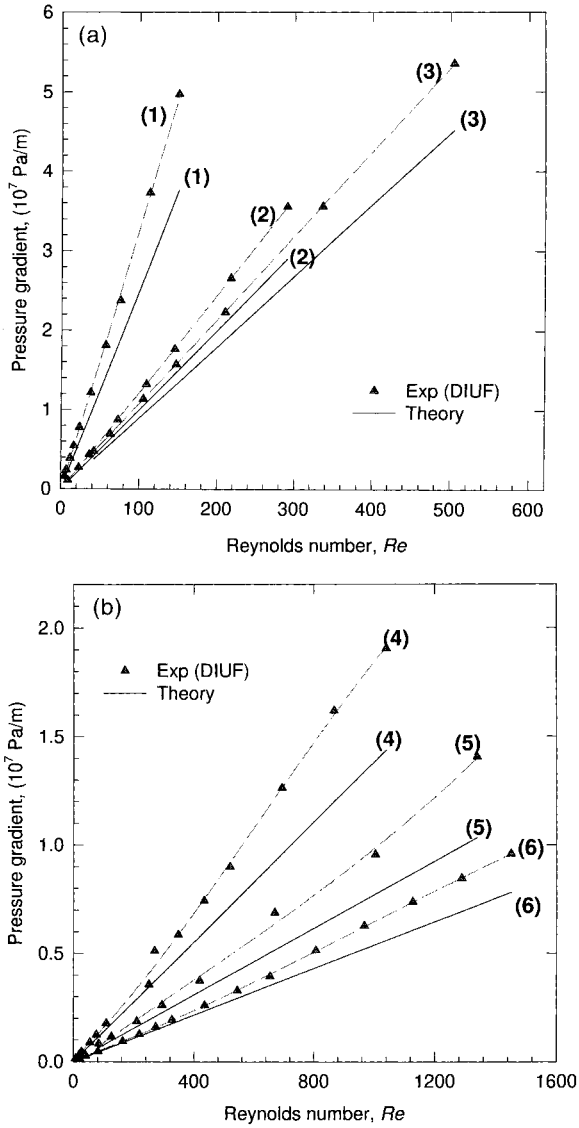

Fig. 5. A comparison of the measured data of pressure gradient vs. Reynolds number with the predictions of conventional laminar flow theory. (a) (1) d_h = 51.3 μm; (2) d_h = 62.3 μm; (3) d_h = 64.9 μm; (b) (4) d_h = 114.5 μm; (5) d_h = 142.0 μm; (6) d_h = 168.9 μm.

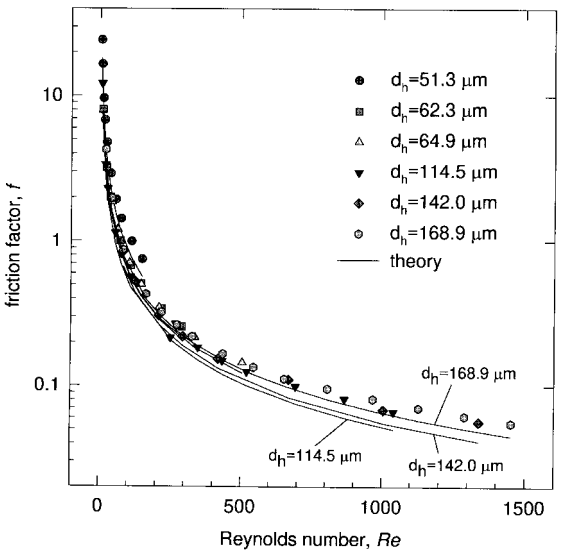

Fig. 6. A comparison of experimentally determined values of friction factor vs. Reynolds number with the predictions of conventional laminar flow theory.

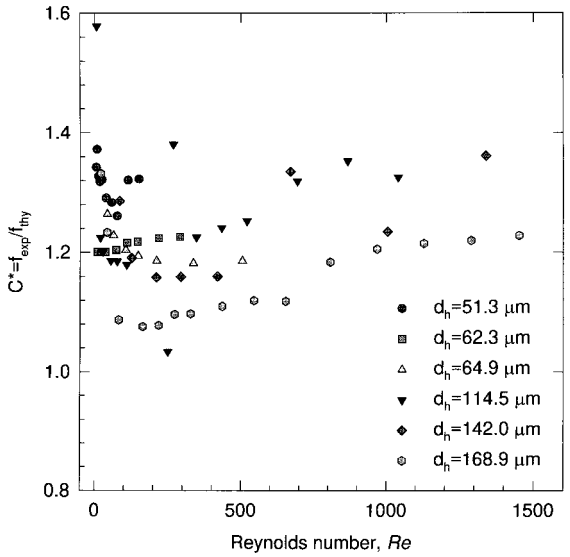

Fig. 7. Friction coefficient ratio vs. *Re*.

3.2. Pressure gradient

For all the microchannels used in this study, the measured pressure gradient P_x is plotted in Fig. 5(a) and (b) as a function of the experimentally determined Reynolds number. For each measured pressure gradient, the theoretical Reynolds number is calculated from the conventional theory. A comparison between the experimental data and theoretically predicted curves is shown in Fig. 5(a) and (b).

As seen in Fig. 5(a) and (b), the theoretical curves are all linear as required by conventional laminar flow theory. It can also be observed that all theoretically predicted curves fall below the experimental curves, which means that at a given flow rate, a higher pressure gradient is required to force the liquid to flow through those microchannels than the predictions of the conventional laminar flow theory. For smaller microchannels, as shown in Fig. 5(a), similar to the linear curves predicted by the conventional theory, the experimental P_x–Re relationships are essentially linear as well. However, the slopes of the measured P_x–Re relationships are approximately 18–32% higher than those of the theoretical curves. For these smaller channels, P_x–Re relationships at higher Reynolds number are not available since the channels will break at high pressure as mentioned before. In Fig. 5(b), the slopes of the experimental P_x–Re relationships for three larger microchannels are also higher than that of the corresponding theoretical curves. It can be seen that in low Reynolds number range, the measured P_x–Re relationships are basically linear. However, as Re increases over 400 or 500, the slopes of these experimental curves start to increase. The slopes of the measured P_x–Re relationships increase from 2% at low Re range to 45% at high Re range, in comparison with the slopes predicted by the classical theory.

3.3. Flow friction

The flow behavior of water through microchannels can be further interpreted in terms of the flow friction. The experimental friction factor f_{exp} can be determined by Eq. (4). In Fig. 6, f_{exp} is plotted as a function of the experimentally determined Reynolds number. For comparison, the relationships between friction factor and Reynolds number predicted by the conventional theory are also plotted in Fig. 6. From Fig. 6, it can be seen that in the high Reynolds number range, all the experimentally determined friction factors are above the theoretical curves, which means for a given Reynolds number, the flow friction in microchannels are higher than the predictions from the conventional theory.

Another important parameter used to describe the flow friction in channels is the friction factor constant C_{f}, which is the product of the friction factor and Reynolds number. It is well known from the conventional laminar flow theory that the friction factor constant for a trapezoidal channel is dependent only on the geometry of the channel cross-section [12]. Hence, for a given trapezoidal channel, a constant value of C_{f} should be expected. However, according to the experimental data in our study, it is found that $C_{\text{f}_{\text{exp}}}$ is no longer a constant for flow in a microchannel. In order

to illustrate the dependence of $C_{f_{exp}}$ on other factors, the friction factor constant ratio C^* is introduced here and defined as

$$C^* = \frac{C_{f_{exp}}}{C_{f_{thy}}} \tag{14}$$

If the experiment Reynolds number and the theoretical Reynolds number are chosen to have the same value, C^* denotes the ratio of experimental friction factor to theoretical friction factor.

$$C^* = \frac{f_{exp}}{f_{thy}} \tag{15}$$

C^* is plotted as a function of Reynolds number in Fig. 7. As can be seen from Fig. 7, C^* is always greater than one. We conclude that the flow friction in the microchannels is 8–38% higher than the theoretical prediction in the Reynolds number range in this study, and depends on the microchannels' hydraulic diameters and Reynolds number.

3.4. Roughness-viscosity model

The above discussed characteristics of higher flow friction have to do with the scale of the microchannels. We measured the surface roughness of the microchannels. The surface roughness of the pyrex glass covers was measured by a Tencor surface profilemeter (TSP). It was found that the surfaces of the pyrex glass covers are very smooth and the average surface roughness is in the order of 10 nm. The average surface roughness of the silicon surface was measured by a high resolution inverted research metallurgical microscope (Olympus, model: PMG3). It varies from 0.8 μm for smaller microchannels to 2 μm for larger microchannels as shown in Table 1. The roughness of such an order of magnitude can be safely neglected if the dimensions of the flow channel are above the order of millimeters. However, for microchannels used in this study, the ratio of $2k/d_h$ ranges from 2.4% to 3.5%. The channels height is the smallest dimension for these trapezoidal microchannels. As seen from Table 1, the ratio of $2k/h$ ranges from 3.4% to 5.7%. Therefore, the surface roughness may have profound effects on the velocity field and the flow friction in microchannels.

The presence of surface roughness affects the laminar velocity profile and decreases the transitional Reynolds number. This has been shown by a number of experiments and a comprehensive review can be found elsewhere [9,14]. Based on Merkle's modified viscosity model, Mala and Li [7] suggested a roughness viscosity model and applied it to explain the effects of the surface roughness on laminar flow in microtubes. Generally, the presence of the surface roughness increases the momentum transfer in the boundary layer near the wall. This additional momentum transfer can be accounted for by introducing a roughness viscosity μ_R in a manner similar to the eddy-viscosity concept in the turbulent flow model. It should be noted that Mala and Li's [8] model was developed for the microtube which has a circular cross-section. In this paper this roughness-viscosity model is further developed for the flow in trapezoidal microchannels.

According to the concept of the roughness viscosity, μ_R should have a higher value near the wall and gradually diminish as the distance from the wall increases; μ_R should also increase as Re increases. The ratio of the roughness viscosity to the fluid viscosity in trapezoidal microchannels is therefore proposed to take the following form:

$$\frac{\mu_R}{\mu} = A\, Re_k \frac{(R_h - l_{min})}{k} \left(1 - \exp\left(-\frac{Re_k}{Re}\frac{(R_h - l_{min})}{k}\right)\right)^2 \tag{16}$$

where A is a coefficient which has to be determined by the experimental data; R_h is defined as the hydraulic radius of the microchannel, which is half of the channel hydraulic diameter; l_{min} is the shortest distance from the point to the silicon surface; Re_k denotes the local roughness Reynolds number and is defined as [9]

$$Re_k = \frac{U_k \rho k}{\mu} \tag{17}$$

where U_k denotes the velocity at the top of the roughness element and is given by [9])

$$U_k = \left(\frac{\partial u}{\partial n}\right)_{\Gamma} k \tag{18}$$

By introducing the roughness viscosity in the equation of motion in a manner similar to the eddy viscosity in the turbulent flow, the equation of motion for laminar flow through a trapezoidal channel becomes

$$\frac{\partial^2 u}{\partial y^2} + \frac{\partial^2 u}{\partial z^2} = \frac{1}{(\mu + \mu_R)}\frac{dP}{dx} \tag{19}$$

with no-slip boundary condition on the wall

$$u(y, z) = 0 \text{ on } \Gamma \tag{20}$$

Eq. (19) is a modified equation of motion that accounts for the effects ofsurface roughness on a laminar flow. Comparing Eq. (19) with Eq. (7), it is apparent that once the roughness viscosity μ_R is known, the

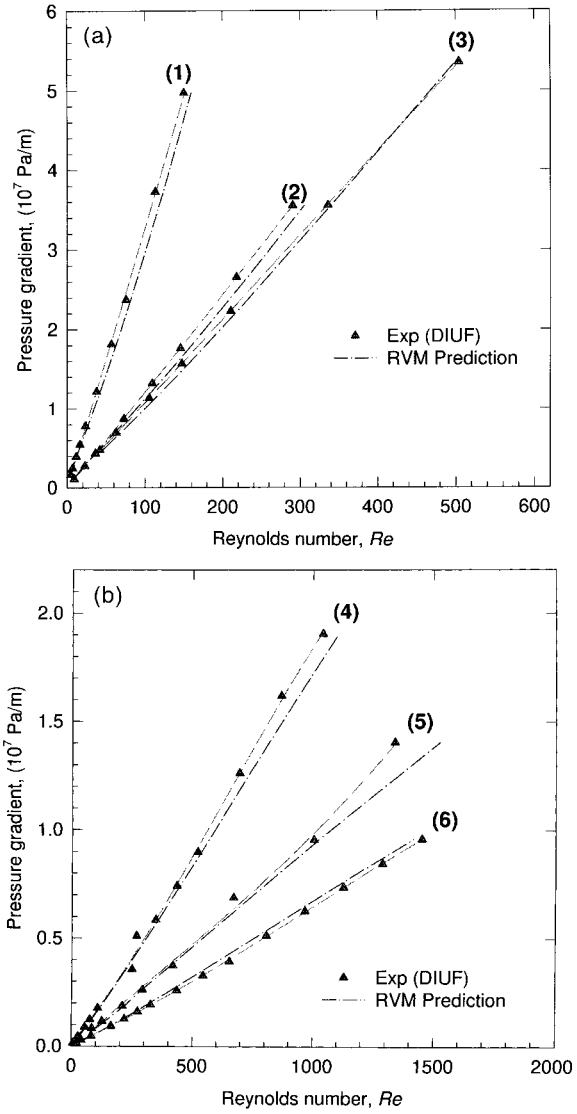

Fig. 8. A comparison of experimental data of pressure gradient vs. Reynolds number with the predictions of the roughness-viscosity model: (a) (1) $d_h = 51.3$ μm; (2) $d_h = 62.3$ μm; (3) $d_h = 64.9$ μm; (b) (4) $d_h = 114.5$ μm; (5) $d_h = 142.0$ μm; (6) $d_h = 168.9$ μm.

modified equation of motion can be solved similarly by the method developed in the previous section.

As seen from the roughness-viscosity function, Eq. (16), all parameters except the coefficient A in Eq. (16) can be determined from the flow field, the dimensions and the average surface roughness of the microchannel. Basically, the coefficient A not only depends on the factors mentioned above, but also depends on the shape and the distribution of the roughness elements. In principle, the A value should vary from channel to channel. However, based on the experimental data, an empirical relation used to calculate the A value can be found by means of numerical approaches. The detailed information about how to determine the empirical relation for A can be found elsewhere, [7]. For the trapezoidal silicon microchannels used in this study, the coefficient A can be evaluated by

$$A = 5.8\left(\frac{R_h}{k}\right)^{0.35} \exp\left(Re^{0.94}\left(5.0\times10^{-5}\frac{R_h}{k} - 0.0031\right)\right) \quad (21)$$

Fig. 8(a) and (b) show the comparison of the measured P_x–Re relationships with the predictions of the roughness viscosity model. As can be seen clearly from Fig. 8(a) and (b), the curves predicted by the roughness viscosity model and the experimental curves are in a good agreement with each other. This implies that the roughness-viscosity model proposed in the present work may be used to interpret the flow characteristics in these microchannels.

4. Summary

Fluid flow in trapezoidal silicon microchannels was experimentally investigated. The results were first compared with conventional theory. It is found that pressure gradient and flow friction in microchannels are higher than that predicted by the conventional laminar flow theory. In a low Re range, the measured pressure gradient increases linearly with Re. When $Re \geq 500$, the slope of P_x–Re relationship increases with Re. It was also found that the friction coefficient for a given microchannel is no longer a constant; the friction coefficient varies with Re. A roughness-viscosity model was proposed in this paper to interpret the experimental data. A good agreement between the experimental data and the model predictions were found.

Acknowledgement

The authors wish to acknowledge the support from a Research Grant of the Natural Science and Engineering Research Council of Canada.

Appendix. Experimental uncertainty analysis

According to Holman [5], if R is a given function of the independent variables $x_1, x_2, x_3, \ldots x_n$, $R = R(x_1, x_2, x_3, \ldots x_n)$, and $w_1, w_2, w_3, \ldots w_n$, are the uncertainties in these inde-

pendent variables, the uncertainty of R can be evaluated by

$$w_R = \left[\left(\frac{\partial R}{\partial x_1}w_1\right)^2 + \left(\frac{\partial R}{\partial x_2}w_2\right)^2 + \ldots + \left(\frac{\partial R}{\partial x_n}w_n\right)^2\right]^{\frac{1}{2}} \tag{A.1}$$

Eq. (A.1) can be further written as

$$\frac{w_R}{R} = \left[\left(\frac{1}{R}\frac{\partial R}{\partial x_1}w_1\right)^2 + \left(\frac{1}{R}\frac{\partial R}{\partial x_2}w_2\right)^2 + \ldots + \left(\frac{1}{R}\frac{\partial R}{\partial x_n}w_n\right)^2\right]^{\frac{1}{2}} \tag{A.2}$$

Based on the instruments and methods employed in our experiments, the uncertainties of our basic measured parameters are evaluated as following.

$$w_a = 0.8\ \mu\text{m} \tag{A.3}$$

$$w_b = 0.8\ \mu\text{m} \tag{A.4}$$

$$w_h = 0.8\ \mu\text{m} \tag{A.5}$$

$$\frac{w_L}{L} = 0.01 \tag{A.6}$$

$$\frac{w_Q}{Q} = 0.02 \tag{A.7}$$

$$\frac{w_{\Delta P}}{\Delta P} = 0.01 \tag{A.8}$$

$$\frac{w_T}{T} = 0.008 \tag{A.9}$$

From Eq. (A.2) and Eqs. (A.3)–(A.9), the uncertainties of some dependent parameters can be evaluated. For the cross-section area of the microchannels,

$$A_c = \frac{(a+b)h}{2} \tag{A.10}$$

$$\frac{w_{A_c}}{A_c} = 0.028 \tag{A.11}$$

For the perimeter of the microchannels,

$$P_c = a + b + 4\sqrt{h^2 + \frac{(a-b)^2}{4}} \tag{A.12}$$

$$\frac{w_{P_c}}{P_c} = 0.0054 \tag{A.13}$$

For the hydraulic diameter of the microchannels,

$$d_h = \frac{4A_c}{P_c} \tag{A.14}$$

$$\frac{w_{d_h}}{d_h} = 0.0285 \tag{A.15}$$

The above provides enough information to estimate the uncertainties of the final experimental results. The pressure gradient P_x, Reynolds number Re, and friction factor f are related to the basic measured parameters by Eqs. (2)–(4). From Eq. (A.2), their uncertainties are evaluated as

$$\frac{w_{P_x}}{P_x} = 0.014 \tag{A.16}$$

$$\frac{w_{Re}}{Re} = 0.046 \tag{A.17}$$

$$\frac{w_f}{f} = 0.076 \tag{A.18}$$

References

[1] S.B. Choi, R.R. Barren, R.O. Warrington, Fluid flow and heat transfer in micro tubes, ASME DSC 40 (1991) 89–93.

[2] R.P. Benedict, Fundamentals of Pipe Flow, John Wiley & Son, New York, 1980.

[3] S.M. Flockhart, R.S. Dhariwal, Experimental and numerical investigation into the flow characteristics of channels etched in ⟨100⟩ silicon, Transactions of the ASME: J. Fluids Engng 120 (1998) 291–295.

[4] J. Harley, H. Bau, Fluid flow in micron and submicron size channels, IEEE Trans. THO249-3 (1989) 25–28.

[5] J.P. Holman, Experimental Methods for Engineers, 4th ed., McGraw-Hill, New York, 1984 .

[6] J.G. Knudsen, D.L. Katz, Fluid Dynamics and Heat Transfer, McGraw-Hill, New York, 1958 .

[7] G.M. Mala, D. Li, Flow characteristics of water in microtubes, Int. J. Heat and Fluid Flow 20 (1999) 142–148.

[8] G.M. Mala, Ph.D. thesis, University of Alberta, 1999.

[9] C.L. Merkle, T. Kubota, D.R.S. Ko, An analytical study of the effects of surface roughness on boundary-layer transition, AF Office of Scien. Res. Space and Missile Sys. Org. AD/A004786, 1974.

[10] X.F. Peng, G.P. Peterson, B.X. Wang, Frictional flow characteristics of water flowing through rectangular microchannels, Experimental Heat Transfer 7 (1994) 249–264.

[11] J.N. Pfahler, Liquid transport in micron and submicron size channels, Ph.D. thesis, Department of Mechanical Engineering and Applied Mechanics, University of Pennsylvania, 1992.
[12] R.K. Shah, A.L. London,, Laminar flow forced convection in ducts, A source book for compact heat exchanger analytical data, Suppl. 1, Academic Press, New York, 1978.
[13] V.L. Streeter, E.B. Wylie, Fluid Mechanics, 8th ed., McGraw-Hill, New York, 1985.
[14] I. Tani, Boundary Layer Transition, Annual Reviews of Fluid Mechanics, vol. I, Annual Reviews, Palo Alto, CA, 1969.
[15] P.Y. Wu, W.A. Little, Measurement of friction factor for flow of gases in very fine channels used for microminiature Joule–Thompson refrigerators, Cryogenics 24(8) (1983) 273–277.
[16] D. Yu, R. Warrington, R. Barren, T. Ameel, An experimental and theoretical investigation of fluid flow and heat transfer in microtubes, Proceedings of the ASME/JSME Thermal Engineering Conference, ASME, 1 (1995) 523–530.